Balancing Sodiophilicity and Mechanical Stability: Sn-Engineered Multicomponent Alloy Interfaces for Anode-Free Sodium Metal Batteries

Yuju Qi,[a] Zewei Hu,[a] Haiying Lu,[a] Zhenwei Tang,[a] Jiayao Wang,[a] Chao Han,[b] Weijie Li*[a]

[a] Y. Qi, Z. Hu, H. Lu, Z. Tang, J. Wang, W. Li
Powder Metallurgy Research Institute
Central South University
Changsha, 410083, China
E-mail: li-306@csu.edu.cn

[b] C Han
School of Materials Sciences and Engineering
Central South University
Changsha, 410083, China

1. Experimental Section

1.1 Material synthesis

MA-$Sn_{0.2}$, MA-$Sn_{0.4}$, MA-$Sn_{0.6}$, MA-$Sn_{0.8}$, and MA-Sn_1 were prepared at room temperature using a coprecipitation strategy. In a typical synthesis, 4 mmol of $Na_4[Fe(CN)_6]$ and 85 mmol of NaCl were dissolved in 50 mL of deionized water to give solution A. In parallel, 0.5 mmol of $SnCl_2$ together with a total of 2 mmol of transition-metal precursors ($FeCl_2 \cdot 4H_2O$, $NiCl_2 \cdot 6H_2O$, $CuCl_2 \cdot 2.5H_2O$, and $CoCl_2 \cdot 6H_2O$, 0.5 mmol each) were dissolved in another 50 mL of deionized water to form solution B. Both solutions were magnetically stirred for 30 min. Afterwards, solution A was added dropwise into solution B under continuous stirring, affording a mixed suspension (solution C). The mixture was allowed to react for 2 h, after which the solid product was isolated by centrifugation, washed repeatedly with deionized water, and finally redispersed in 40 mL of deionized water under ultrasonication to obtain solution D. In a separate step, 0.2 g of CNTs were dispersed in deionized water by ultrasonic treatment. Subsequently, 5 mL of solution D was introduced into the CNT dispersion, and the mixture was ultrasonicated for 1 h to promote uniform loading. The resulting suspension was filtered under vacuum, and the collected solid was dried at 60 °C. The dried precursor was gently ground, spread uniformly in a quartz boat, and subjected to thermal treatment in a tube furnace: the temperature was increased to 800 °C at 5 °C min^{-1} under flowing Ar and maintained for 2 h. The final product obtained under these conditions was designated as MA-$Sn_{0.2}$. The MA-Sn_0, MA-$Sn_{0.4}$, MA-$Sn_{0.6}$, MA-$Sn_{0.8}$, and MA-Sn_1 samples were synthesized following the same protocol, with the Sn content adjusted to the desired level.

1.2 Preparation of electrode

The as-prepared active materials and PVDF binder were first blended and ground thoroughly at a mass ratio of 8:2. A suitable amount of N-methyl-2-pyrrolidone (NMP) was then introduced to obtain a uniform slurry, which was subsequently deposited onto aluminum foil using an ultrasonic spray-coating process.

1.3 Preparation of $Na_3V_2(PO_4)_3$ cathode

$Na_3V_2(PO_4)_3$ powder, CNTs, and PVDF binder were first combined in a mass ratio of 8:1:1 and thoroughly ground to obtain a uniform mixture. A suitable amount of N-methyl-2-pyrrolidone (NMP) was then added to prepare a well-dispersed slurry, which was evenly applied onto a carbon-coated aluminum foil current collector. After drying, the resulting electrodes were punched into 10 mm-diameter discs for subsequent measurements.

2. Materials Characterization

A field-emission scanning electron microscope (FE-SEM, JEOL JSM-6700) equipped with an energy-dispersive X-ray spectroscopy (EDS) detector was employed to examine the morphologies and elemental distributions of MA-Sn0.2, MA-Sn0.4, MA-Sn0.6, MA-Sn0.8, and MA-Sn1. X-ray diffraction (XRD) patterns were recorded on a Bruker D8 diffractometer using Cu Kα radiation at a scan rate of 10° min^{-1}. The microstructures of MA-$Sn_{0.2}$ and MA-Sn_1 were further investigated by transmission electron microscopy (TEM, JEOL 4000EX). In situ visualization of Na deposition on MA-$Sn_{0.2}$, MA-$Sn_{0.4}$, MA-$Sn_{0.6}$, MA-$Sn_{0.8}$, and MA-Sn_1 substrates was performed using an optical microscope (Star-micro T2-M100) under a constant deposition current density of 1 mA cm^{-2}. The carbon content was analyzed using a thermogravi-metric analyzer (TGA, METTLER Toledo TGA-DSC 3+) at a heating rate of 10 1C min^{-1}.

3. Electrochemical Measurements

All 2032-type coin cells were fabricated in a high-purity Ar glove box, where the concentrations of H_2O and O_2 were both maintained below 0.1 ppm. Galvanostatic tests were performed on a Neware multichannel battery tester (CT-4008Tn-5V10mA-HWX, Shenzhen, China). Unless otherwise stated, 1 M $NaPF_6$ in diglyme (G2) was used as the electrolyte for the Na-based cells. Asymmetric cells were configured with a Na metal foil (14 mm in diameter) as the counter/reference electrode and MA-Sn_x (x = 0.2-1) discs (16 mm in diameter) as the working electrodes. A polypropylene separator (Celgard 2500) and 50 μL of electrolyte were employed in each cell. The long-term Coulombic efficiency (CE) was determined by repeatedly stripping Na at current densities of 1 and 2 mA cm^{-2} to a fixed areal capacity of 1 mAh cm^{-2}, followed by plating back until the cell voltage reached 0.5 V. For symmetric cells, a defined amount of Na was first electrodeposited onto the MA-Sn_x substrates to obtain Na/MA-Sn_x electrodes, which were then assembled face-to-face. Their electrochemical impedance spectra were collected at different temperatures using a 10 mV AC perturbation over a frequency range of 1 MHz-100 mHz. The activation energy for ion transport was calculated from Arrhenius plots according to k=Ae-Ea/RT, where k is the rate constant, R is the gas constant, and T is the absolute temperature. Tafel polarization curves were recorded on an electrochemical workstation between -0.1 and 0.1 V at a scan rate of 1 mV s^{-1}. The Tafel plots were derived from polarization curves based on the Tafel equation ($\eta = a + b \log i$), where η is the overpotential and i is the current density. The Tafel slope was obtained from the linear fitting region, and the exchange current density (i_0) was determined by extrapolating the fitted line to zero overpotential. MA-$Sn_{0.6}$||NVP pouch cells were operated within 2.2-3.8 V. They were first activated at a low rate of 0.05 C and then subjected to cycling at 0.5 C for further performance evaluation.

4. Supplementary Figures

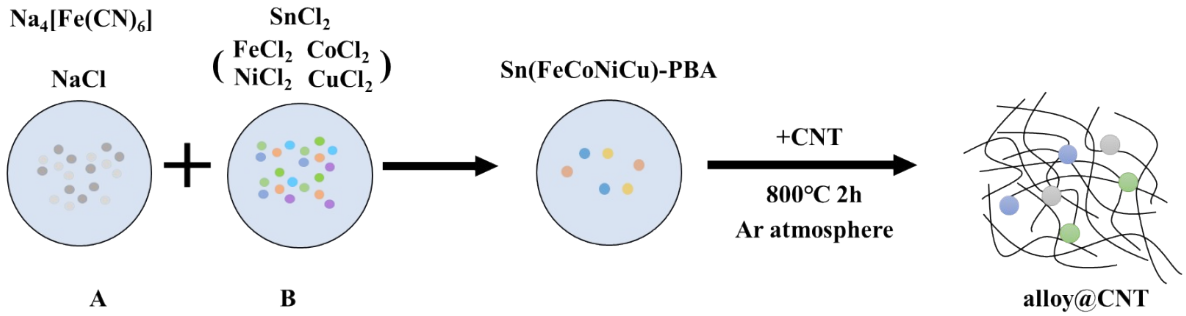

Figure S1 The synthesis processes of MA-$Sn_{0.2}$, MA-$Sn_{0.4}$, MA-$Sn_{0.6}$, MA-$Sn_{0.8}$, and MA-Sn_1 materials.

Five metal chlorides (Fe, Co, Ni, Cu, Sn) were used as precursors to form Prussian blue analogues via a room-temperature co-precipitation in aqueous solution. After adding carbon nanotubes (CNTs) and ultrasonic dispersion, the mixture was dried and thermally reduced in Ar to obtain alloy nanoparticles anchored on CNTs.

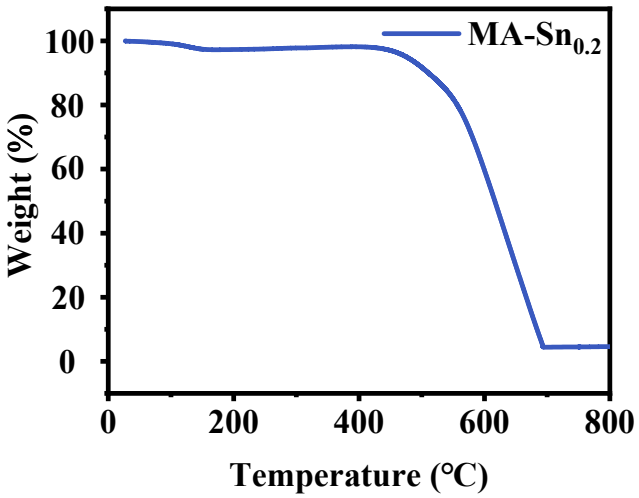

Figure S2 TGA of MA-$Sn_{0.2}$.

The results of thermogravimetric analysis confirmed that alloy nanoparticles accounted for 5% of the material.

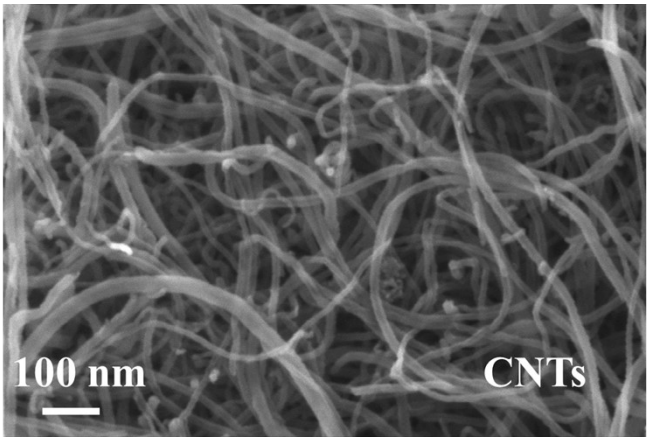

Figure S3 SEM of CNTs.

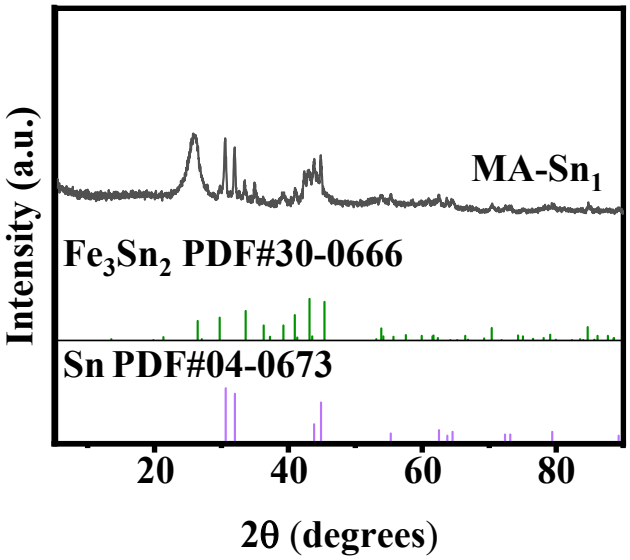

Figure S4 XRD of MA-Sn_1.

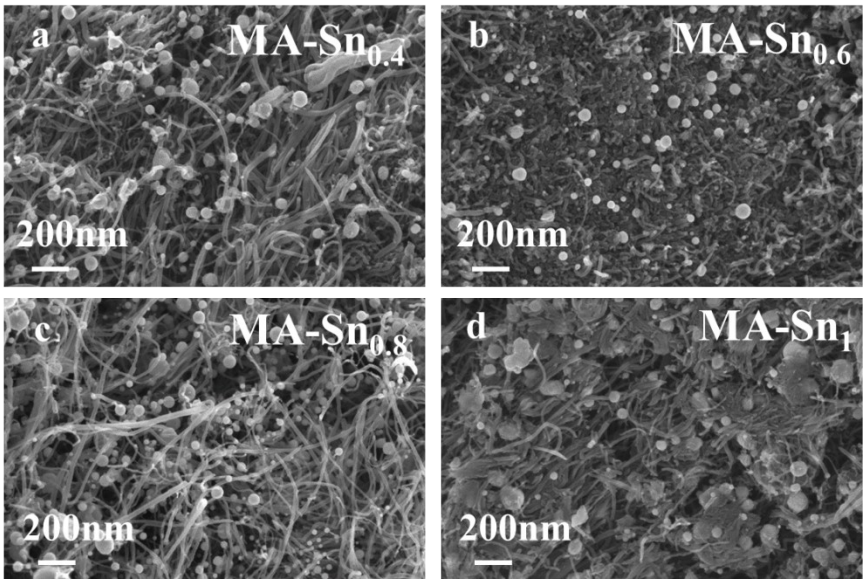

Figure S5 SEM images of (a) MA-$Sn_{0.4}$, (b) MA-$Sn_{0.6}$, (c) MA-$Sn_{0.8}$, and (d) MA-Sn_1.

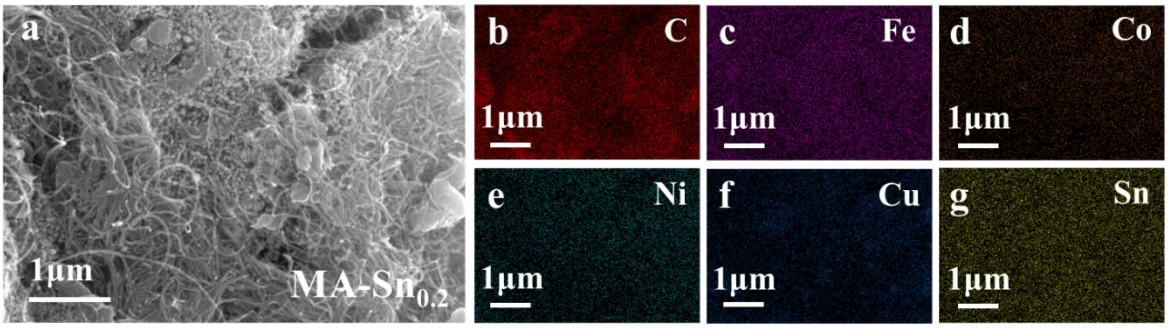

Figure S6 (a) SEM of MA-$Sn_{0.2}$ and corresponding elemental distribution of (b) C, (c) Fe, (d) Co, (e) Ni, (f) Cu, and (g) Sn.

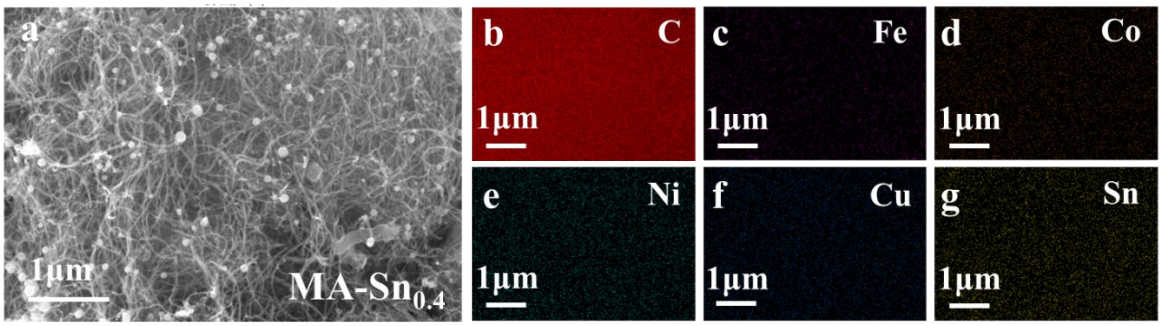

Figure S7 (a) SEM of MA-$Sn_{0.4}$ and corresponding elemental distribution of (b) C, (c) Fe, (d) Co, (e) Ni, (f) Cu, and (g) Sn.

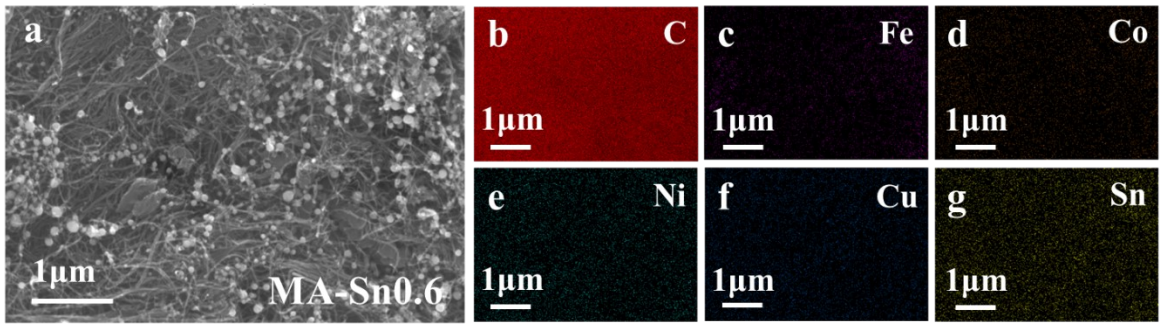

Figure S8 (a) SEM of MA-$Sn_{0.6}$ and corresponding elemental distribution of (b) C, (c) Fe, (d) Co, (e) Ni, (f) Cu, and (g) Sn.

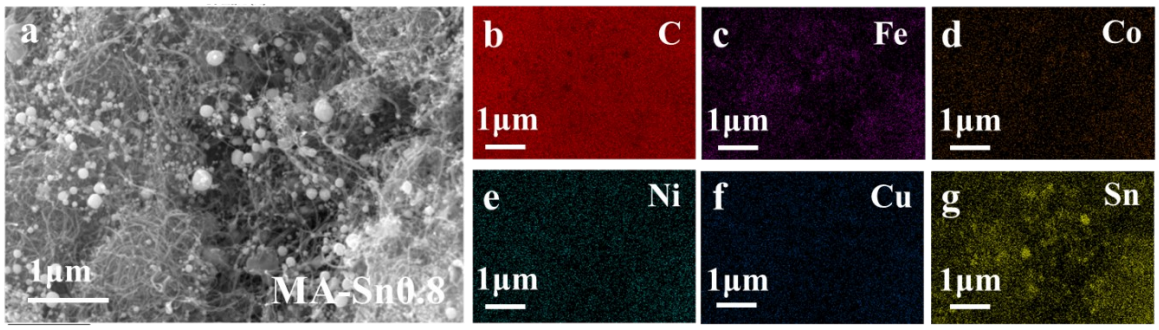

Figure S9 (a) SEM of MA-$Sn_{0.8}$ and corresponding elemental distribution of (b) C, (c) Fe, (d) Co, (e) Ni, (f) Cu, and (g) Sn.

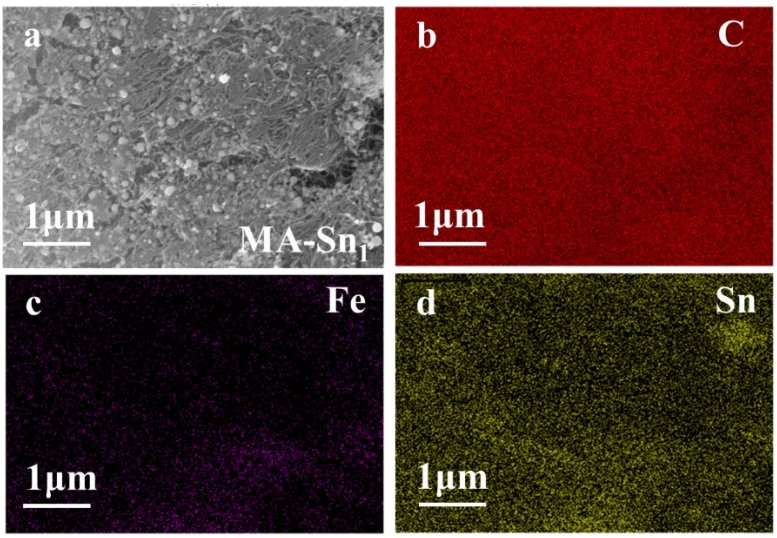

Figure S10 (a) SEM of MA-Sn_1 and corresponding elemental distribution of (b) C, (c) Fe, (d) Sn.

1 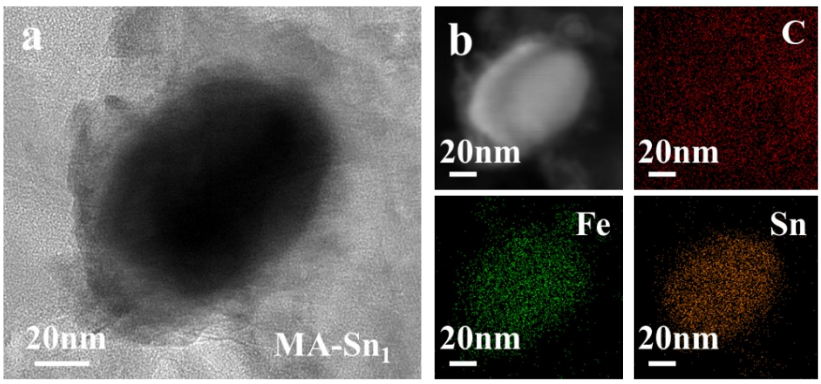

2 Figure S11 (a) TEM of MA-Sn_1 and corresponding elemental distribution of (b) C, Fe, and Sn.

3

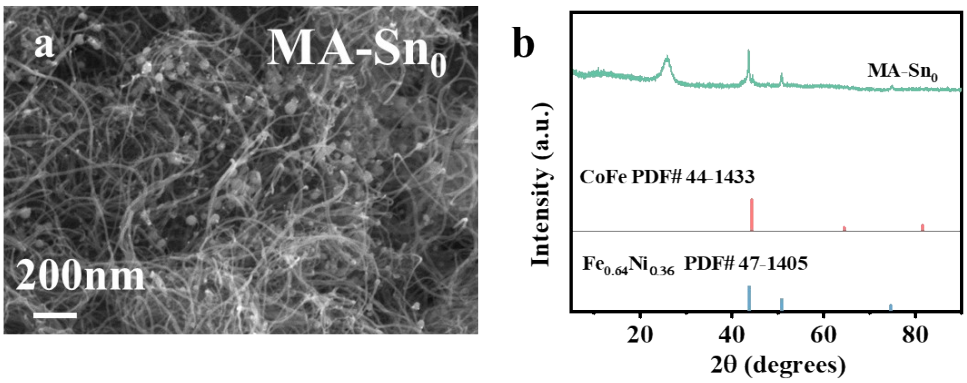

1

2 Figure S12 SEM and XRD of MA-Sn_0.

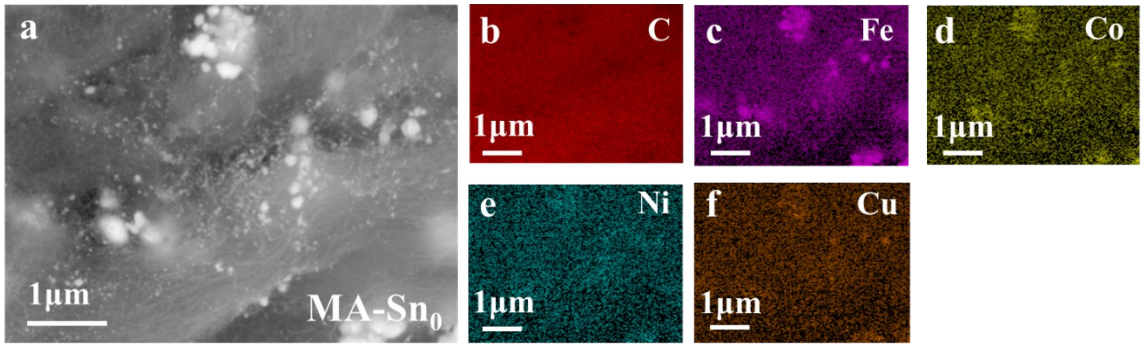

3

4 Figure S13 SEM of MA-Sn_0.

5

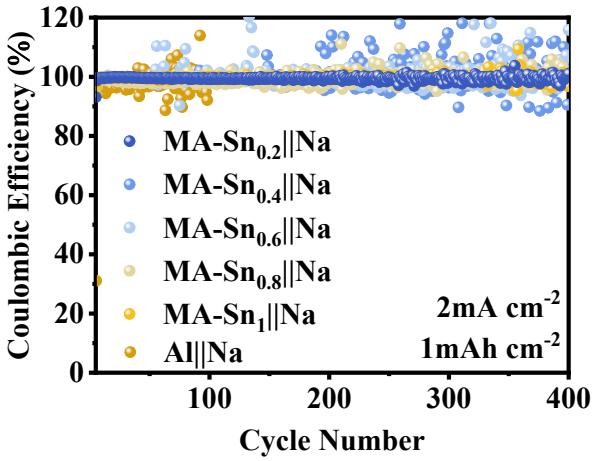

Figure S14 CE profiles of asymmetric cells at 2mA cm^{-2} of 1mAh cm^{-2}.

The excellent reproducibility further supports the reliability of the observed performance differences among MA-Sn_x samples.

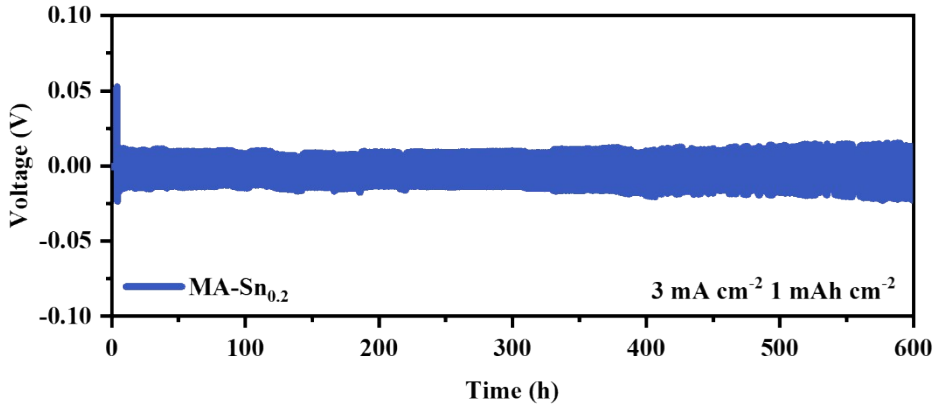

Figure S15 Cycling performance of symmetric cells under 3 mA cm^{-2} of 1mAh cm^{-2}.

At 3 mA cm^{-2} and 1 mAh cm^{-2}, it maintains regular voltage profiles for over 600 h.

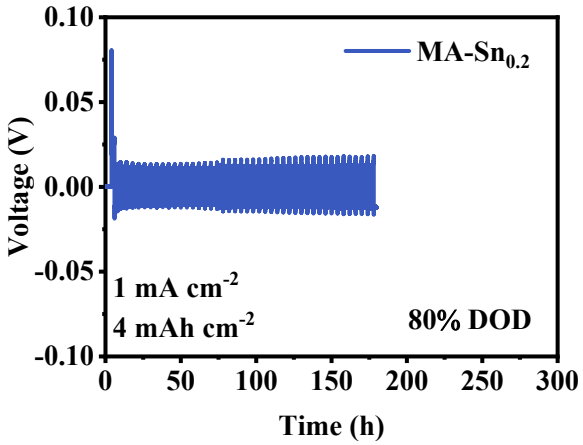

Figure S16 Cycling performance of MA-$Sn_{0.2}$ symmetric cells at 1 mA cm^{-2} of 4 mAh cm^{-2}.

Even under higher DOD conditions, MA-$Sn_{0.2}$ maintains relatively stable cycling.

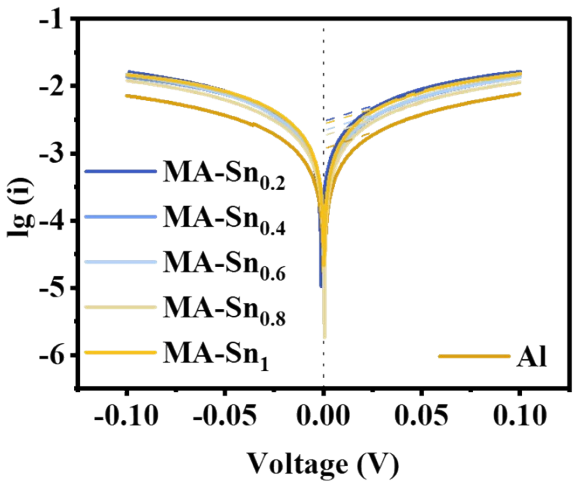

Figure S17 Tafel profile of different substrates.

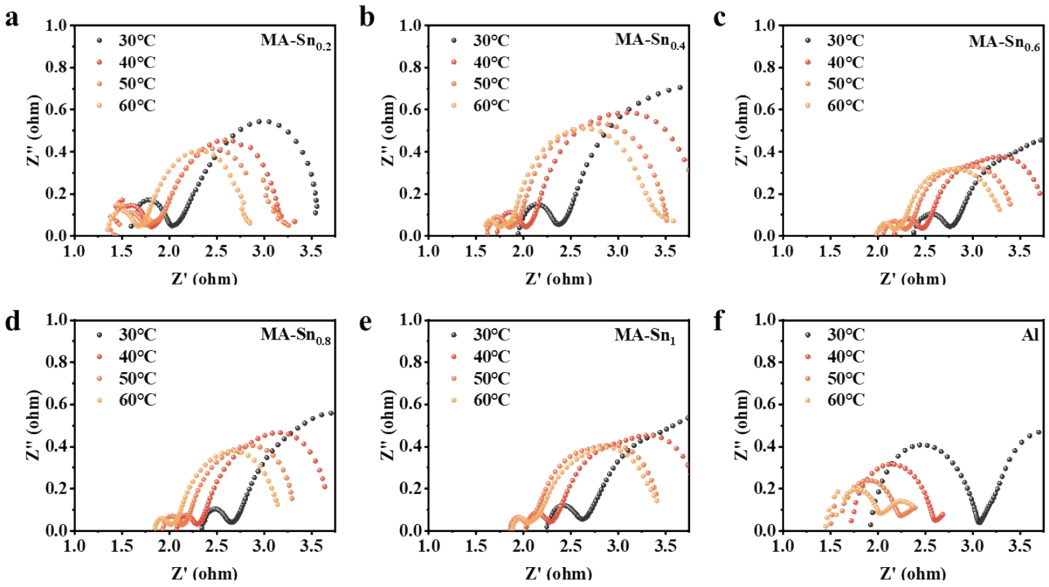

Figure S18 The EIS spectra of symmetric cells at different temperatures.

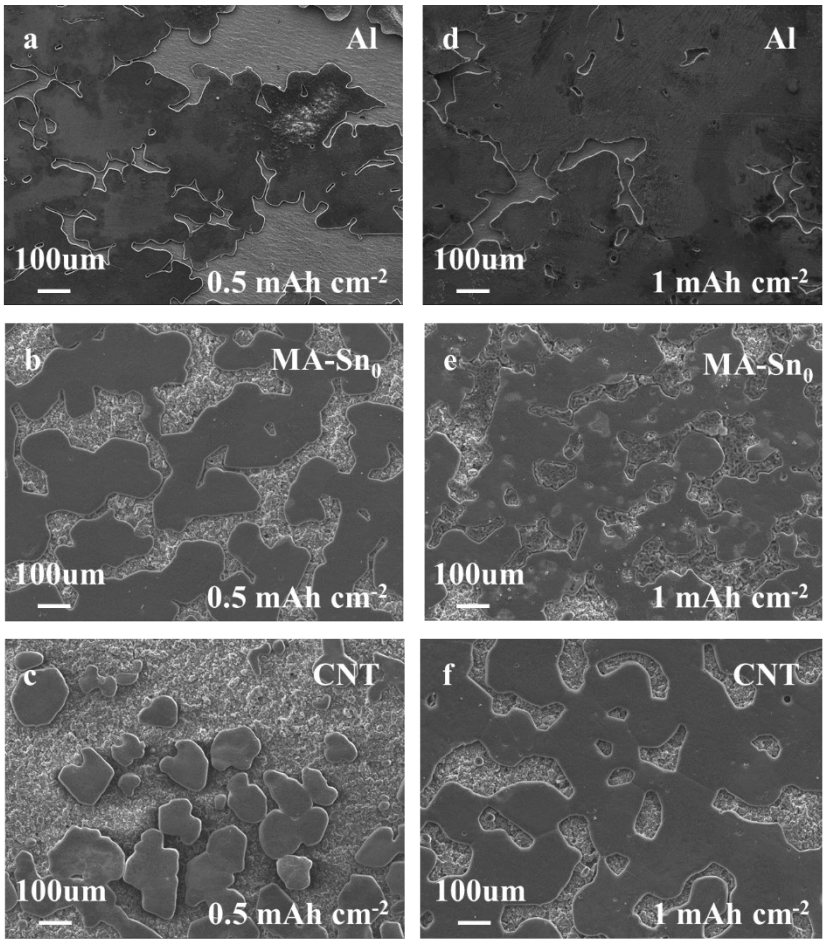

Figure S19 SEM images of (a, d) Al, (b, e) MA-Sn_0, and (c, f) CNT current collector with different Na deposition capacities.

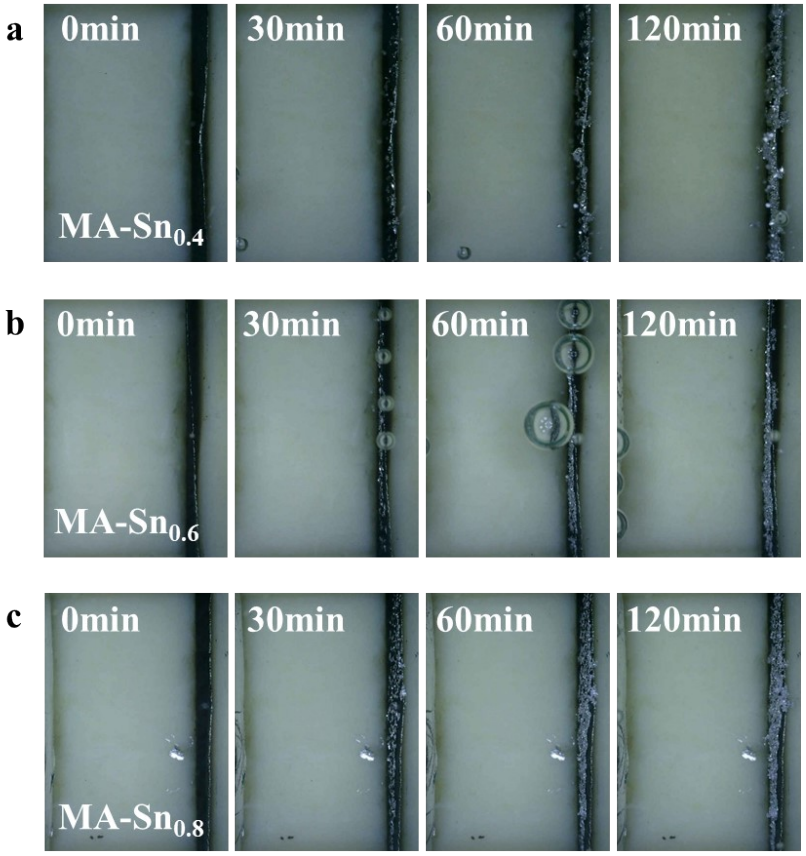

Figure S20 In-situ optical microscopy observations of the Na plating process on the (a) MA-$Sn_{0.4}$, (b) MA-$Sn_{0.6}$, and (c) MA-$Sn_{0.8}$.

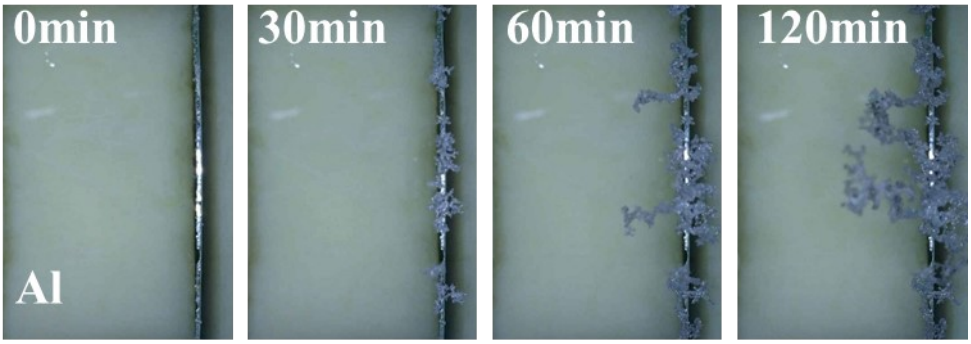

Figure S21 In-situ optical microscopy observations of the Na plating process on the Al.

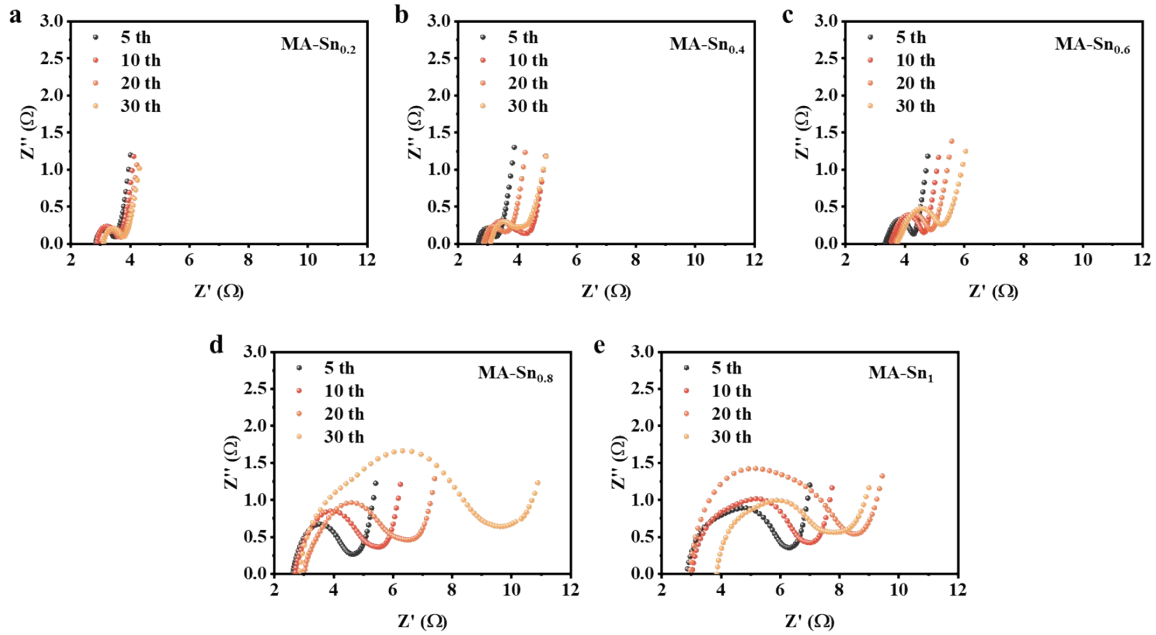

Figure S22 The EIS spectra of asymmetric cells at different cycles.

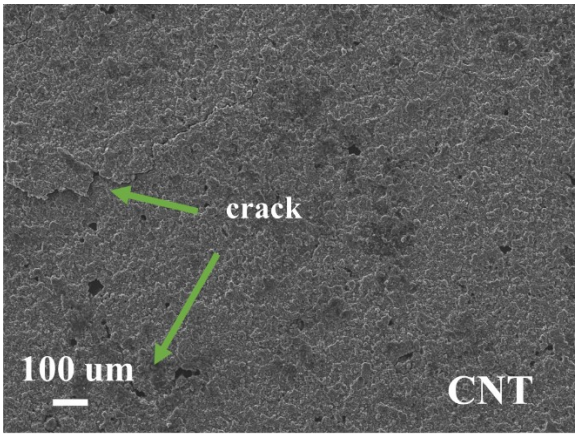

Figure S23 SEM of CNT after cycling.

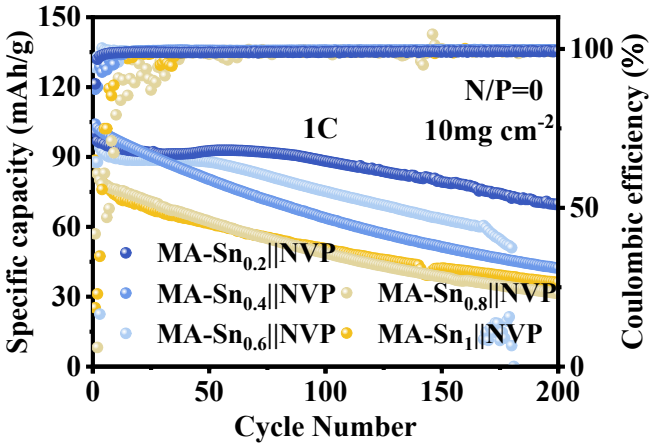

Figure S24 Cycling performance of MA-Sn_x||NVP (x = 0.2, 0.4, 0.6, 0.8, and 1) anode-free cells at 1 C.

Even at a high cathode loading of 10 mg cm^{-2}, MA-$Sn_{0.2}$ still delivered superior cycling performance at 1 C.